J. Fluid Mech. (1997), *vol.* 331, *pp.* 81–106

On the propagation of internal bores

By JOSEPH B. KLEMP, RICHARD ROTUNNO AND WILLIAM C. SKAMAROCK
National Center for Atmospheric Research, Boulder, CO 80307, USA

(Received 18 January 1996 and in revised form 29 July 1996)

According to classical hydraulic theory, the energy losses within an external bore must occur within the expanding layer. However, the application of this theory to describe the propagation of internal bores leads to contradiction with accepted gravity-current behaviour in the limit as the depth of the expanding layer ahead of the bore becomes small. In seeking an improved expression for the propagation of internal bores, we have rederived the steady front condition for a bore in a two-layer Boussinesq fluid in a channel under the assumption that the energy loss occurs within the contracting layer. The resulting front condition is in good agreement with available laboratory data and numerical simulations, and has the appropriate behaviour in both the linear long-wave and gravity-current limits. Analysis of an idealized internal bore assuming localized turbulent stresses suggests that the energy within the expanding layer should, in fact, increase. Numerical simulations with a two-dimensional non-hydrostatic model also reveal a slight increase of energy within the expanding layer and suggest that the structure of internal bores is fundamentally different from classical external bores, having the opposite circulation and little turbulence in the vicinity of the leading edge. However, if there is strong shear near the interface between layers, the structure and propagation of internal jumps may become similar to their counterparts in classical hydraulic theory. The modified jump conditions for internal bores produce some significant alterations in the traditional Froude-number dependence of Boussinesq shallow-water flow over an obstacle owing to the altered behaviour of the upstream-propagating internal bore.

1. Introduction

Internal bores arise in a variety of atmospheric situations when disturbances are generated along a pre-existing inversion layer. For example, observations suggest that bores may arise from the interaction of inversion layers with fronts (cf. Clarke, Smith & Reid 1981, on the Morning Glory in Northern Australia), with thunderstorm outflows (cf. Schreffler & Binskowski 1981; Haase & Smith 1984, on disturbances in the Central US), and with coastally trapped disturbances (cf. Dorman 1987; Hermann *et al.* 1990, in events along the west coast of the USA). These internal bores may be revealed by propagating pressure jumps or roll clouds along their leading edge, and thus bear some resemblance to classical hydraulic bores propagating in a single-layer fluid. According to single-layer hydraulic theory, the height h_f and speed U of the bore are governed by the conservation of mass and momentum within the layer, which requires an accompanying loss of energy (cf. Stoker 1957, p. 316). Imposing these same constraints on bores forming in a shallow layer beneath a semi-infinite medium of finite density reproduces the classical hydraulic jump conditions, except with gravity replaced by a suitably reduced gravity g' (cf. Turner 1973, p. 67). In a Boussinesq fluid,

however, this theory is in contradiction with known gravity-current behaviour; as the layer depth ahead of the bore h_a vanishes, the speed of a finite-height bore tends to infinity rather than to a finite speed such as that derived by Benjamin (1968). For internal bores, the theoretical underpinnings of the classical theory are problematic since the fluid above the denser layer can participate in the redistribution of both momentum and energy across the bore.

In the present study, we rederive the front condition for a bore propagating in a two-layer Boussinesq fluid using assumptions that are consistent with Benjamin's (1968) theory for gravity-current behaviour when the layer depth ahead of the jump vanishes. To this end, we assume that energy loss occurs in the contracting layer (the layer above an inversion in atmospheric situations) instead of within the expanding (lower) layer as dictated by classical hydraulic theory. Comparisons with available laboratory data in §2 suggest that this new front condition may provide an improved characterization of internal-bore propagation relative to previous theory for large values of h_f/h_a, and converges to the conventional hydraulic theory in the linear long-wave limit ($h_f/h_a \to 1$). An analysis in §3 including the first-order effects of localized mixing supports our assumptions, and demonstrates that the energy within the expanding layer may, in fact, increase. In §4, we reconsider the dam-break problem for the case in which a semi-infinite layer of the denser fluid initially extends out ahead of the dam, and demonstrate that hydraulic solutions together with the new front condition are in good agreement with two-dimensional non-hydrostatic simulations.

Shocks propagating into a quiescent fluid are typically called bores, while flows decelerating through a nearly stationary shock are termed hydraulic jumps. When there is negligible density in the medium above a shallow-water flow (such as air over a layer of water), there is no distinction between bores and hydraulic jumps other than perhaps the coordinate frame of reference (cf. Stoker 1957, pp. 324–326). However, in a Boussinesq fluid, internal hydraulic jumps may have substantially different behaviour from bores if strong shear exits along the interface between two layers of differing density ahead of the jump. This situation may arise, for example, with hydraulic jumps forming in the lee of obstacles, where accelerated flow within the layer adjacent to the obstacle creates strong shear in the vicinity of the layer interface. We investigate the behaviour of internal jumps in the presence of shear in §5 through additional simulations with the two-dimensional non-hydrostatic model. These results suggest that strong shear ahead of the jump may significantly alter the flow structure and turbulent stresses near the leading edge of the jump, resulting in propagation that agrees better with the classical hydraulic theory in which energy loss is confined to the expanding layer.

The behaviour of steady shallow-water hydraulic flow of speed U over an obstacle is characterized by two dimensionless parameters: the ratio of the maximum obstacle height to the upstream depth of the shallow-water layer h_0, and the upstream Froude number $F = U/(g'h_0)^{1/2}$. The regimes for formation of upstream-propagating bores and lee hydraulic jumps were derived by Houghton & Kasahara (1968), and have been used widely in interpreting geophysical flows. In §6, we rederive the regime diagram for steady Boussinesq flow over an obstacle using the modified front condition proposed in §2. Interestingly, in the revised diagram, the hysteresis zone described by Baines & Davies (1980), in which the flow ahead of the obstacle either remains supercritical or develops an upstream-propagating bore depending on the history of the flow, disappears. Our summary comments are included in §6.

2. Internal bore in a channel

To analyse the propagation of an internal bore, we consider the simplified system of a steady two-layer fluid in a channel. In a coordinate framework moving with the leading edge of the bore, a uniform flow having velocity U in both layers approaches from the right as illustrated in figure 1 (for simplicity, we assume the right-to-left flow in the figure has positive velocity). The density is assumed constant within each of the two immiscible layers, and the denser lower layer is the expanding layer in passing through the bore.

The steady horizontal momentum equation can be expressed as:

$$\frac{\partial \rho u^2}{\partial x}+\frac{\partial \rho uw}{\partial z}+\frac{\partial p}{\partial x}=\frac{\partial \tau_{xx}}{\partial x}+\frac{\partial \tau_{xz}}{\partial z}, \tag{1}$$

where (u, w) are velocity components in the (x, z)-coordinates, τ represents the turbulent shear stress, and p is the pressure. In this two-layer system, the momentum is no longer conserved within the layer beneath the bore; rather, conservation of momentum now requires that the overall flow force, integrated vertically over the channel depth, be conserved across the bore. Integrating (1) across the bore from a point r far ahead of the leading edge (to the right in figure 1) to a point l far behind, and over the channel depth d, the stress terms vanish (assuming zero-stress wall conditions and that turbulent fluctuations are weak far downstream) and the flow-force balance becomes:

$$\int_0^d (p_r+\rho U^2)\,\mathrm{d}z=\int_0^d (p_l+\rho u_l^2)\,\mathrm{d}z. \tag{2}$$

Far upstream and downstream of the bore, the flow is hydrostatic, such that $\partial p_1/\partial z=-g\rho_1$ and $\partial p_2/\partial z=-g\rho_2$ in the lower and upper layers, respectively. Assuming that within each layer the mass is conserved and the velocity becomes uniform far downstream, (2) becomes:

$$\left[-\frac{h_a}{h_f}+\frac{\rho_2}{\rho_1}\frac{d-h_a}{d-h_f}\right](h_f-h_a)\,U^2+\tfrac{1}{2}g'(h_f^2-h_a^2)+\frac{d}{\rho_1}\Delta P_d=0, \tag{3}$$

where $\Delta P_d=p_l(d)-p_r(d)$ is the pressure difference across the bore along the top of the channel, and $g'=g(\rho_1-\rho_2)/\rho_1$ represents the reduced gravity.

In the limiting case of an external bore in a one-layer fluid, $\rho_2=0$ and $\Delta P_d=0$, such that

$$\frac{U^2}{g'h_f}=\frac{h_f+h_a}{2h_a}, \tag{4}$$

where here, $g'=g$. In this limit, the momentum within the expanding layer decreases in passing through the bore (reflected by the first term in (3)), while the vertically integrated pressure force across the bore increases.

For internal bores, the density difference between the two layers is often small, and thus we invoke the Boussinesq approximation to simplify the ensuing analysis. In this limit, the manner in which the flow-force balance is satisfied changes dramatically; the momentum integrated across both layers in the channel now increases in traversing the bore (the first term in (3) becomes positive), requiring a decrease in the vertically integrated pressure force across the bore.

The analysis of a steady internal bore in a two-layer fluid also reveals an ambiguity not present in the analysis of classical external bores. Yih & Guha (1955) found that

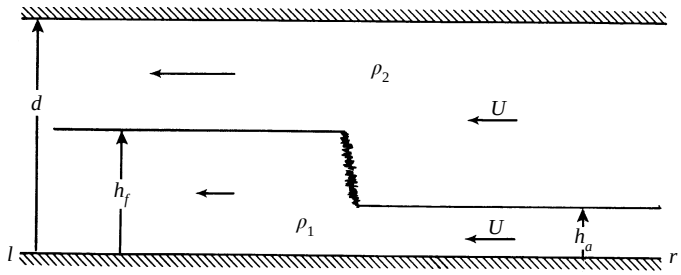

FIGURE 1. Schematic of an internal bore in a two-layer fluid within a channel in a coordinate framework moving at the bore speed U.

imposing mass conservation in each layer together with overall conservation of momentum leaves the solution for the bore speed U in terms of the bore height undetermined to a constant; an additional constraint is required relating the downstream pressure to upstream conditions. They obtained solutions by evaluating the momentum balance within each layer, neglecting the stress terms along the fluid interface, and approximating the pressure along the interface by the average of its value far upstream and downstream such that:

$$\int_r^l p_1(h_1)\frac{\partial h_1}{\partial x}\,\mathrm{d}x \simeq \tfrac{1}{2}[p_l(h_f)+p_r(h_a)]\,(h_f-h_a), \tag{5}$$

where $h_1(x)$ denotes the height of the interface. Combining the flow-force balance for just the upper layer with (5) yields:

$$\Delta P_d = -\frac{\hat{\rho}(d-h_a)\,(h_f-h_a)}{(d-h_f)\,[d-\frac{1}{2}(h_f+h_a)]}\,U^2. \tag{6}$$

where $\hat{\rho}=\rho_2\simeq\rho_1$. Combining (3) and (6) produces Yih & Guha's expression for the bore speed, which in the Boussinesq limit is given by:

$$\frac{U^2}{g'h_f} = \frac{(d-h_f)\,[d-\frac{1}{2}(h_f+h_a)]\,(h_f+h_a)}{2h_a\,d^2+d(h_f^2-2h_a\,h_f-h_a^2)}. \tag{7}$$

In addressing the closure for this problem, Chu & Baddour (1977) and Wood & Simpson (1984) followed the analogy with open channel hydraulic flow and assumed that all the energy loss occurs within the lower (expanding) layer. This approach is also consistent with Schijf & Schönfeld's (1953) suggestion that for an internal bore, energy should be conserved within the layer that is relatively accelerated in traversing the bore. Applying the Bernoulli equation across the bore within the upper layer:

$$\Delta P_d = \tfrac{1}{2}\hat{\rho}\left[1-\frac{(d-h_a)^2}{(d-h_f)^2}\right]U^2, \tag{8}$$

which, combined with (3) in the Boussinesq limit, yields Wood & Simpson's (1984) relation for bore propagation:

$$\frac{U^2}{g'h_f} = \frac{(d-h_f)^2(h_f+h_a)}{d(h_f^2+2h_a\,d-3h_a\,h_f)}. \tag{9}$$

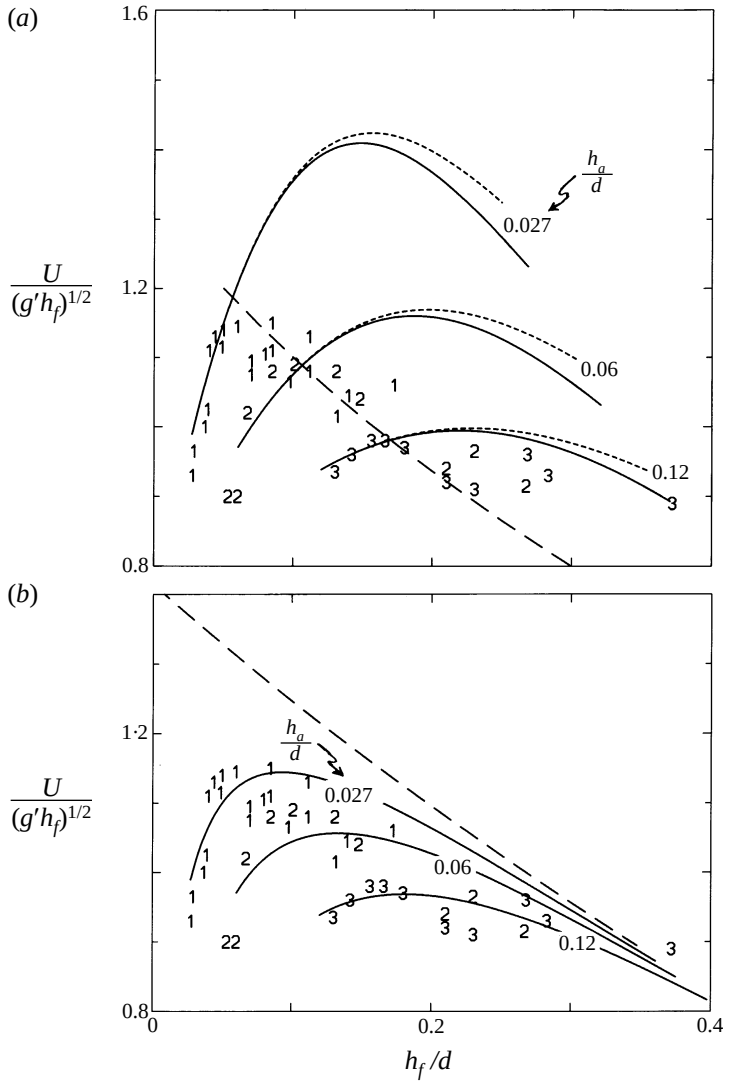

FIGURE 2. Theoretical curves and experimental data for the propagation of a steady internal bore in a channel for $h_a/d = 0.027$, 0.06, and 0.12. The corresponding laboratory data from Wood & Simpson (1984) are labelled 1, 2 and 3, respectively. (*a*) Theoretical bore speed proposed by Wood & Simpson (1984) (equation (9), displayed with solid lines) and by Yih & Guha (1955) (equation (7), displayed with short dashed lines). The long-dashed line represents experimental results for a gravity current obtained by Simpson & Britter (1979). (*b*) Theoretical bore speed assuming all energy loss occurs in the upper (contracting) layer. The long-dashed curve denotes Benjamin's (1968) curve for gravity-current propagation.

Wood & Simpson also carried out laboratory experiments to measure the speed of bores propagating in a two-layer Boussinesq fluid in a channel for comparison with (9). Their results are displayed in figure 2(*a*) for three different depths of the lower layer ahead of the bore. The theoretical profiles for each h_a/d begin at $h_f = h_a$ and continue to the right with increasing h_f, terminating at the point where conditions behind the bore become just critical (cf. Klemp, Rotunno & Skamarock 1994). As the height of the bore increases, the theoretical bore speeds begin to substantially overpredict the observed speeds, particularly for the smaller values of h_a/d. Recognizing that a bore

should not propagate faster than a gravity current of equivalent height h_f, Wood & Simpson also included an experimental curve for gravity–current propagation obtained by Simpson & Britter (1979), and proposed that this curve be considered an upper bound for (9). However, this restriction precludes the use of (9) over a large portion of the range of possible bore heights. The expression (7) derived by Yih & Guha (1955) predicts bore speeds very similar to those of Wood & Simpson.

The contradictions of the above-described theories with accepted gravity-current behaviour in the limit as $h_a \to 0$ are well illustrated for the case in which the channel depth becomes large. In this limit ($d \to \infty$), both (7) and (9) reduce to the classical behaviour for an external bore indicated by (4). As the depth of the layer ahead of the bore becomes small, the bore speed increases without bound rather than asymptoting to a constant gravity-current speed, such as $(2g'h_f)^{1/2}$ as proposed by Benjamin (1968).

To resolve this inconsistency with gravity-current behaviour, we propose an alternative derivation for the speed of an internal bore assuming energy loss occurs in the upper layer as proposed by Benjamin (1968) for gravity currents. Therefore, in contrast with classical hydraulic theory, we assume that energy is conserved within the lower layer. With this approach, applying the Bernoulli equation along the bottom of the channel yields:

$$\frac{\Delta P_d}{\hat{\rho}} = \frac{1}{2}\left[1 - \frac{h_a^2}{h_f^2}\right] U^2 - g'(h_f - h_a). \tag{10}$$

Using (10) together with (3), the Boussinesq front condition becomes:

$$\frac{U^2}{g'h_f} = \frac{h_f(d-h_f)(2d-h_f-h_a)}{d(h_f d + h_a d + h_f^2 - 3h_a h_f)}. \tag{11}$$

Evaluating (11) in the extremes for h_f/h_a,

$$\frac{U^2}{g'h_f} = \frac{(d-h_f)}{d} \quad \text{as} \quad \frac{h_f}{h_a} \to 1, \tag{12}$$

$$\frac{U^2}{g'h_f} = \frac{(2d-h_f)(d-h_f)}{d(d+h_f)} \quad \text{as} \quad \frac{h_f}{h_a} \to \infty, \tag{13}$$

which captures the appropriate limiting behaviour for both linear long-wave (cf. Turner 1973, p. 18) and gravity-current (Benjamin 1968) propagation as h_f/h_a approaches one and infinity, respectively. (We originally explored the use of (11) in the Boussinesq dam-break problem as a front condition for the disturbances propagating back into the reservoir (Klemp *et al.* 1994). In that situation, the front condition must approach the gravity-current limit (13) when the initial reservoir spans the entire channel depth (the lock-exchange problem) in order to achieve the desired symmetric behaviour of the upstream and downstream propagating disturbances.)

Comparing (11) with Wood & Simpson's (1984) experimental data in figure 2(*b*) reveals good agreement across a broad range of h_a/h_f. In the limit of large channel depth, (11) becomes:

$$\frac{U^2}{g'h_f} = \frac{2h_f}{h_f + h_a} \quad \text{as} \quad d \to \infty, \tag{14}$$

which, as $h_a \to 0$, produces the familiar gravity–current result, in contrast to the singular behaviour that arises in (4).

Laboratory experiments conducted by Rottman & Simpson (1989) further document

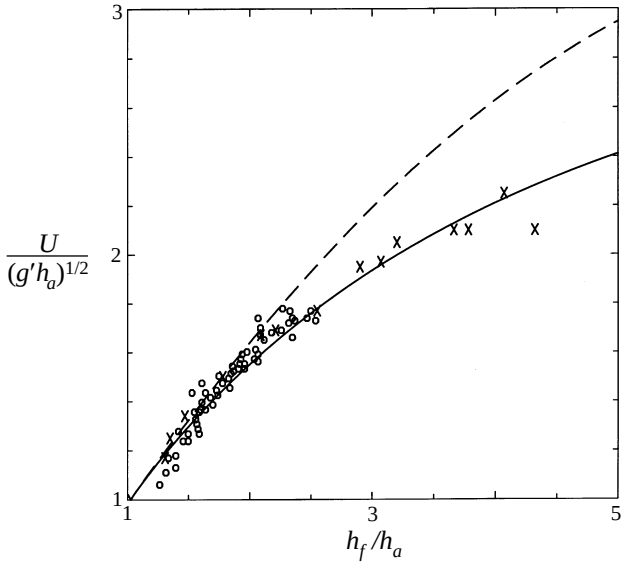

FIGURE 3. Internal bore speed (normalized by the layer depth h_a ahead of the bore) as a function of bore height in a channel with $h_a/d = 0.035$. Data of: $\times$, Rottman & Simpson (1989); $\bigcirc$, Baines (1984). ——, Theoretical bore speed (11) assuming energy loss occurs in the upper layer. – – –, Speed from (9) assuming the energy loss is confined to the lower layer.

the speed of internal bores as displayed in figure 3 (using their dimensionless variables). Over the range of h_f/h_a produced in the experiments, they observed three types of bore structures: for $h_f/h_a < 2.3$, the bore was undular and laminar; for $2.3 < h_f/h_a < 3.5$, the bore remained undular, with turbulence mixing behind the first crest; while for $h_f/h_a > 3.5$, the bore resembled the head of a gravity current. In spite of these variations in bore structure, the theoretical bore speed (11), conserving energy within the lower layer, provides a reasonable fit to the data over the entire range of observed bore heights.

Baines (1994) summarizes the theories proposed by Yih & Guha (1955) and by Chu & Baddour (1977) and Wood & Simpson (1984) in his discussion of two-layer hydraulic jumps, and dismisses the plausibility of neglecting energy loss in the expanding layer since it yields predictions that differ significantly from the other two approaches. We have included data from Baines' (1984) laboratory experiments in figure 3 for $h_a/d = 0.035$, recognizing that with $\rho_2/\rho_1 = 0.79$ in these experiments, the fluids may not be entirely Boussinesq. Over the range of bore heights reported ($h_f/h_a \leqslant 2.5$), our theory (11), assuming energy conservation within the lower layer, fits the data at least as well as (9), and is clearly superior for the larger values of h_f/h_a obtained by Rottman & Simpson (1989).

The overall energy loss in the Boussinesq system corresponding to energy conservation in the lower layer $E_u = \hat{\rho} U(d-h_a)\, g' \Delta_u$ is readily obtained by evaluating the head loss Δ_u in the Bernoulli equation evaluated across the top of the channel, with the result:

$$E_u = \frac{\hat{\rho} U^3 d(d-h_a)(d-2h_f)(h_f-h_a)^3}{2h_f^2(d-h_f)^2(2d-h_f-h_a)}. \tag{15}$$

As expected, E_u reduces to Benjamin's (1968) result for gravity currents as $h_a \to 0$. Since $E_u \to 0$ as $h_f \to h_a$, it is perhaps not surprising that (11) also has the correct form (12) in the inviscid gravity-wave limit.

Following the same procedure, the overall energy loss $E_l = \hat{\rho} U h_a g' \Delta_l$ realized when energy is conserved in the upper layer can be expressed as:

$$E_l = \frac{\hat{\rho} U^3 h_a \, d(d-2h_f)\,(h_f-h_a)^3}{2h_f^2(d-h_f)^2(h_f+h_a)}, \tag{16}$$

which is equivalent to the expression derived by Wood & Simpson (1984). E_l has the same behaviour as E_u as $h_f \to h_a$, but $E_l \to 0$ in the gravity-current limit as $h_a \to 0$. As demonstrated by Benjamin (1968), steady inviscid solutions in this gravity–current limit are possible only in the special circumstance when $h_f = \frac{1}{2}d$. Wood & Simpson also derived the expression for energy change within an internal bore subject to Yih & Guha's (1955) assumption and point out that this approach implies an energy gain in the upper layer.

3. Implications of localized mixing

In the analyses discussed above, assuming the velocity within a fluid layer does not vary with height far behind the bore requires that the energy loss is also uniformly distributed across the layer. However, laboratory observations of internal bores (cf. Wood & Simpson 1984) suggest that the turbulence is concentrated in proximity to the interface between the layers of differing density. Consequently, the energy within a layer may change even though a significant portion of the layer is effectively inviscid.

We explore here some of the implications of localized turbulent mixing by modifying the uniform-flow model to allow head loss that is confined to the vicinity of the interface between the layers. The flow along both the top and bottom of the channel is assumed to be inviscid. Far behind the bore, flow within the lower layer has velocity $u_1(z)$, with $u_1(0) = U_1$ along the bottom of the channel, while the upper layer has velocity $u_2(z)$ with $u_2(d) = U_2$ at the top of the channel, as illustrated in figure 4. We assume that mass does not mix across the interface (as in immiscible fluids), and, therefore, mass continuity now requires

$$U_1 = \frac{Uh_a + Q_1}{h_f}, \quad U_2 = \frac{U(d-h_a) + Q_2}{d-h_f}, \tag{17}$$

where Q_1 and Q_2 are the integrated velocity deficits:

$$Q_1 = \int_0^{h_f} (U_1 - u_1)\,\mathrm{d}z, \quad Q_2 = \int_{h_f}^{d} (U_2 - u_2)\,\mathrm{d}z. \tag{18}$$

Applying the Bernoulli equation along both the top and bottom of the channel, and integrating the hydrostatic equation across the channel both far upstream and downstream of the bore, $\Delta P_d = \frac{1}{2}\hat{\rho}(U^2 - U_2^2)$ and

$$U_2^2 - U_1^2 = 2g'(h_f - h_a). \tag{19}$$

In the flow-force balance (2) together with (19), we employ the traditional wake approximation and assume the velocity deficit far behind the bore becomes small, such that terms of order $(U_i - u_i)^2/U_i^2$ (where $i = 1, 2$) may be neglected (cf. Prandtl & Tietjens 1934, p. 125). Retaining the first-order terms for the velocity deficit, (2) and (19) become:

$$\left[\tfrac{1}{2}d - \frac{h_a^2}{h_f} - \frac{(d-h_a)^2}{d-h_f} + \frac{d(d-h_a)^2}{2(d-h_f)^2}\right] U^2 + \frac{d(d-h_a)}{(d-h_f)^2} U Q_2 = \tfrac{1}{2}g'(h_f^2 - h_a^2), \tag{20}$$

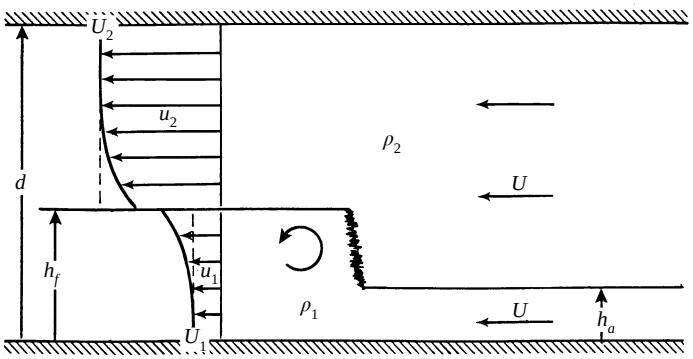

FIGURE 4. Schematic of an internal bore in a two-layer fluid within a channel assuming turbulent mixing is localized in the vicinity of the interface between layers.

and

$$\left[\frac{(d-h_a)^2}{(d-h_f)^2}-\frac{h_a^2}{h_f^2}\right]U^2-\frac{2h_a}{h_f^2}UQ_1+\frac{2(d-h_a)}{(d-h_f)^2}UQ_2=2g'(h_f-h_a), \tag{21}$$

respectively. Combining (20) and (21) yields:

$$\frac{U^2}{g'h_f}=\frac{h_f(d-h_f)(2d-h_f-h_a)+(d-h_f)^2(h_f+h_a)\zeta}{d[h_f d+h_a d+h_f^2-3h_a h_f+(h_f^2+2h_a d-3h_a h_f)\zeta]}, \tag{22}$$

where

$$\zeta=\frac{h_a(d-h_f)}{h_f(d-h_a)}\frac{Q_1}{Q_2}. \tag{23}$$

Note that $\zeta=0$ ($Q_1=0$, conserving energy in the lower layer) recovers (11), while $\zeta\to\infty$ ($Q_2=0$, conserving energy in the upper layer) reduces (22) to (9).

The rate of loss of mechanical energy within each layer is given by:

$$E_1=\int_0^{h_f}u_1[p_r-p_l+\tfrac{1}{2}\hat{\rho}(U^2-u_1^2)+\hat{\rho}g'(z_r-z_l)]\,\mathrm{d}z, \tag{24}$$

$$E_2=\int_{h_f}^{d}u_2[p_r-p_l+\tfrac{1}{2}\hat{\rho}(U^2-u_2^2)]\,\mathrm{d}z. \tag{25}$$

Again neglecting quadratic terms in the velocity deficit leads to:

$$E_1=\hat{\rho}U^2\frac{h_a^2}{h_f^2}Q_1 \tag{26}$$

and

$$E_2=\hat{\rho}U^2\frac{(d-h_a)^2}{(d-h_f)^2}Q_2. \tag{27}$$

From (20), (21), (26) and (27), it can be verified that for $Q_2=0$, $E_1=E_l$, and for $Q_1=0$, $E_2=E_u$. Thus, to this order of approximation, assuming localized mixing leads to the same expressions for both propagation speed and overall energy loss as those derived assuming uniform flow in each layer. This result is similar to that obtained by Klemp

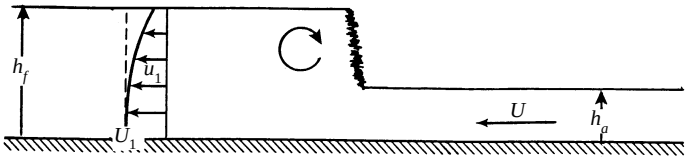

FIGURE 5. Schematic of a classical hydraulic bore with energy loss concentrated near the fluid interface.

et al. (1994) in analysing gravity-current behaviour with localized mixing. (In Klemp *et al.* (1994), the propagation speed and overall energy loss derived assuming localized mixing differed slightly from that obtained with uniformly distributed head loss. This small discrepancy arose because in the analysis with localized mixing, some terms that were quadratic in the velocity deficit were retained.)

Although this analysis contains the same indeterminacy as before (one further constraint is required to determine Q_1/Q_2 in (23)), it now provides guidance in specifying closure for the problem since (26) and (27) dictate that the energy loss must be of the same sign as the velocity deficit within each layer. The flow profile depicted in figure 4 for the lower layer is consistent with the expected influences of shear stresses acting along the interface between the two layers. Since $u_1(z) \geqslant U_1$, the integrated velocity deficit Q_1 is negative, such that the energy in the lower layer (26) must, in fact, increase ($E_1 < 0$).

The absence of energy losses within the expanding layer does not necessarily contradict the observations (cf. Wood & Simpson 1984) that significant turbulence occurs within that layer. In the equation for total kinetic energy, the viscous effects (which qualitatively represent the eddy mixing) can be expressed as the sum of two terms: an energy flux due to internal friction and a dissipation term (Landau & Lifshitz 1959, p. 53). While the dissipation term is always positive, the viscous (eddy) flux of energy between the two layers can be of either sign, and may offset the dissipation term within the expanding layer. An energy gain within the expanding layer reflects an increase in head along streamlines behind the bore, which is to be expected when viscous or turbulent stresses act to accelerate the fluid (Batchelor 1967, p. 266).

Energy loss within the lower layer would require a velocity profile with decreased speed near the interface as indicated in figure 5. This behaviour is observed in classical hydraulic jumps on a free surface (cf. Hager & Bremen 1989; Long *et al.* 1991; Hornung *et al.* 1995), consistent with the observed generation of clockwise vorticity (in the perspective of figure 5). However, for internal bores, shear stresses near the interface, created by baroclinic generation of counterclockwise vorticity (discussed further in §§4 and 5) produces a velocity profile with the qualitative behaviour shown in figure 4, which implies energy gain in the lower layer.

The characteristics of the bore based on this analysis with localized mixing are illustrated in figure 6 for $h_f/h_a = 3$ and $h_a/d \to 0$, obtained by solving (20) and (21) as a function of Q_2. The bore speed and energy loss assuming energy conservation in the upper layer ($Q_2 = 0$) fall along the left-hand edge of the figure, while values corresponding to energy conservation in the lower layer lie along the indicated $Q_1 = 0$ line. (For $h_a/d \to 0$, Yih & Guha's (1955) results are the same as those assuming energy loss only in the lower layer, $Q_2 = 0$.) Between these limits, the energy loss within each layer varies monotonically as a function of Q_2 and the overall energy loss is fairly constant. However, for flow within the lower layer consistent with figure 4, the relevant portion of the figure lies to the right of the $Q_1 = 0$ line, where E_1 is negative. In this

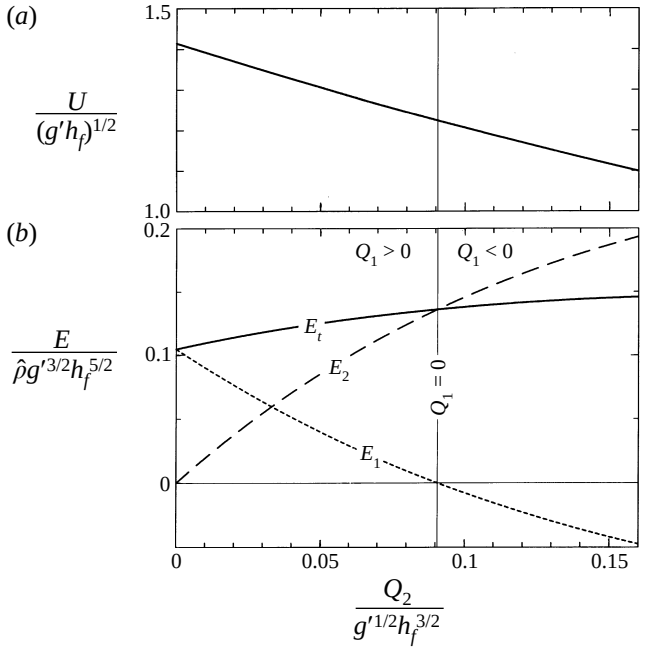

FIGURE 6. (*a*) Speed U and (*b*) energy loss E of bore with localized mixing for $h_f/h_a = 3$ and $h_a/d \to 0$ as a function of the integrated velocity deficit in the upper layer Q_2. In (*b*), $E_t = E_1 + E_2$ represents the total energy loss.

region, the bore speed decreases below that predicted by (11) based on the assumption of energy conservation in the lower layer. The right-hand boundary of figure 6 reflects the value of Q_2 for which $U_1 \to 0$, which is well beyond the conditions of quantitative validity for this analysis.

Based on expectations that $Q_1 < 0$, the assumption $Q_1 = 0$ inherent in our derivation of (11) should be more accurate than the assumption of energy conservation in the contracting layer ($Q_2 = 0$) that requires $Q_1 > 0$. Furthermore, the overall agreement of (11) with the laboratory data evident in figures 2 and 3 suggests that the energy gain within the expanding layer may be negligible in comparison to the magnitude of energy loss in the contracting layer. Therefore, we believe that assuming conservation of energy within the expanding layer is a reasonable approximation in deriving a simple expression for the speed of a steady internal bore.

4. The dam-break problem

To evaluate further the propagation of internal bores, we consider the release of a semi-infinite reservoir of relatively dense fluid of depth h_0 in a channel with a shallower layer of the denser fluid of depth h_a out ahead of the reservoir, as illustrated in figure 7. The dependence of the height and speed of the internal bore on the front condition following removal of the dam is well illustrated in the simple solutions to the one-layer shallow-water layer (SWL) equations using a reduced gravity g', valid in the limit as $d \to \infty$. Following the rightward-moving characteristic $u + 2(g'h)^{1/2}$ from far upstream in the reservoir to a point just behind the downstream-propagating bore provides the expression:

$$2(g'h_0)^{1/2} = (1-\beta)\,U + 2(g'h_f)^{1/2}, \tag{28}$$

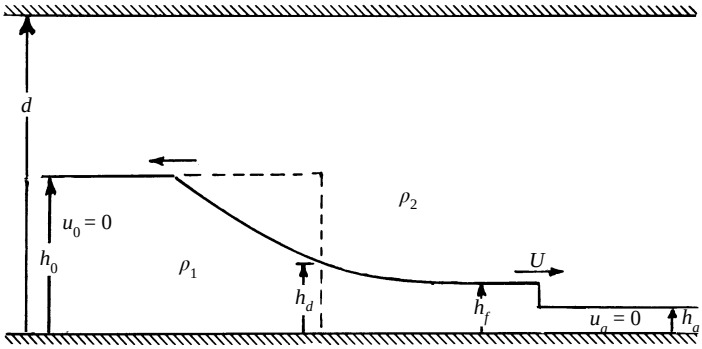

FIGURE 7. Schematic of the dam-break problem in a channel with a shallower layer of the denser fluid ahead of the reservoir.

where $\beta = h_a/h_f$, and $(1-\beta)\,U$ is the fluid velocity just behind the bore. Expressing the front condition in the form $U = k(g'h_f)^{1/2}$ then yields:

$$\frac{U}{(g'h_0)^{1/2}} = \frac{2k}{2+(1-\beta)\,k}, \tag{29}$$

$$\frac{h_f}{h_0} = \left[\frac{2}{2+(1-\beta)\,k}\right]^2, \tag{30}$$

where from (4) and (14),

$$k = \left[\frac{2}{1+\beta}\right]^{1/2}, \quad \text{energy loss above SWL,} \tag{31}$$

or

$$k = \left[\frac{1+\beta}{2\beta}\right]^{1/2}, \quad \text{energy loss within SWL.} \tag{32}$$

Assuming the energy loss occurs above the SWL, $k \to \sqrt{2}$ as $h_a \to 0$, and the front propagates with a speed $U = 0.828(g'h_0)^{1/2}$ maintaining a constant height $h_f = 0.343h_0$. This behaviour is in reasonable quantitative agreement with laboratory experiments (Rottman & Simpson 1983) and numerical simulations (Klemp *et al.* 1994) for a Boussinesq fluid. Using the front condition corresponding to energy loss within the lower layer, $U = 2(g'h_0)^{1/2}$ and the height of the front h_f vanishes as $h_a \to 0$, which is the classical hydraulic solution (cf. Stoker 1957, p. 340). However, this behaviour is not observed in laboratory realizations of the dam-break problem within a Boussinesq fluid (cf. Rottman & Simpson 1983).

For a channel of finite depth, the downstream-propagating disturbances in the two-layer shallow-water system are described by the characteristic equation:

$$h_1\frac{\mathrm{d}u_1}{\mathrm{d}h_1} + \frac{h_1 u_1}{d-h_1} + \left[\frac{g'h_1(d-h_1)}{d} - \frac{h_1 u_1^2}{d-h_1}\right]^{1/2} = 0, \tag{33}$$

where u_1 and h_1 are the speed and height of the lower layer (cf. Rottman & Simpson 1983; Klemp *et al.* 1994). The behaviour of the bore is determined by integrating (33), beginning far upstream in the reservoir where $h_1 = h_0$ and $u_1 = 0$, until the specified front condition is just satisfied. Applying the front condition (11) yields solutions for the speed of the frontal bore shown by the solid lines in figure 8. For $h_a/h_0 \to 1$, the front speed asymptotically approaches the long-wave speed for a two-

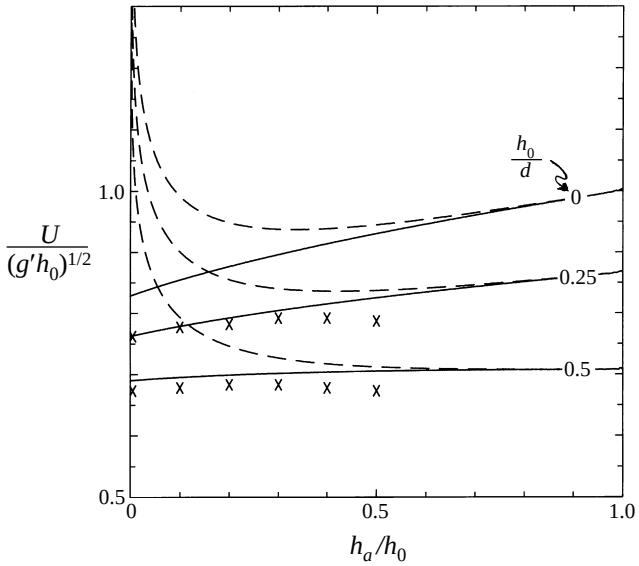

FIGURE 8. Bore speed for the dam-break problem depicted in figure 7 derived from the two-layer shallow-water equations with energy loss ——, occurring in the upper layer and – – –, confined to the lower layer for $h_0/d = 0$, 0.25, and 0.5. ×, Non-hydrostatic model results for $h_0/d = 0.25$, and 0.5.

layer fluid $U = (g'h_0(d-h_0)/d)^{1/2}$, while as $h_a/h_0 \to 0$, the front behaves as a gravity current and satisfies Benjamin's (1968) front condition (see Klemp *et al.* 1994). In contrast, solutions using the front condition (9) that conserves energy in the upper layer (also shown in figure 8), exhibit much higher front speeds in the gravity–current limit.

We also conducted numerical simulations of the dam-break problem using the two-dimensional non-hydrostatic Boussinesq model described in Klemp *et al.* (1994). For atmospheric applications, this model conserves potential temperature for adiabatic flow, and is consistent with the analyses in the previous sections for Boussinesq flow by defining $g' = (\theta_2 - \theta_1)/\theta_2$. In these experiments, the reservoir has an initial height of $h_0 = 5$ km, with a potential temperature θ_1 that is 10 K colder than the surrounding atmosphere at $\theta_2 = 300$ K. A layer of the colder air extends ahead of the dam, having depth h_a ranging from 0 to 2.5 km in the various simulations. In the horizontal direction, the domain dimension is 60 km, and the grid interval is 200 m. Simulations were conducted for $h_0/d = 0.25$ and 0.5 with a vertical grid increment of 100 m, and with free-slip conditions imposed along the upper and lower boundaries.

The nature of the bore resulting from the release of the reservoir is illustrated in figure 9 for several different layer depths ahead of the bore for $h_0/d = 0.25$. In each case, the leading edge of the bore is smooth and turbulence develops through Kelvin–Helmholtz (K–H) instability behind the head with intensity that diminishes as the height of the bore decreases with increasing h_a. As h_a/h_0 is increased much beyond 0.5, the bore becomes undular with little evidence of turbulence.

The speed of the bore in the numerical simulations was estimated by visually aligning the position of the bore in the contour plots at $\hat{t} = 8$ and 16, where $\hat{t} = t(g'/h_0)^{1/2}$ is the dimensionless time. The bore speeds from the various simulations are plotted in figure 8, and provide confirmation for the shallow-water model that conserves energy within the lower layer.

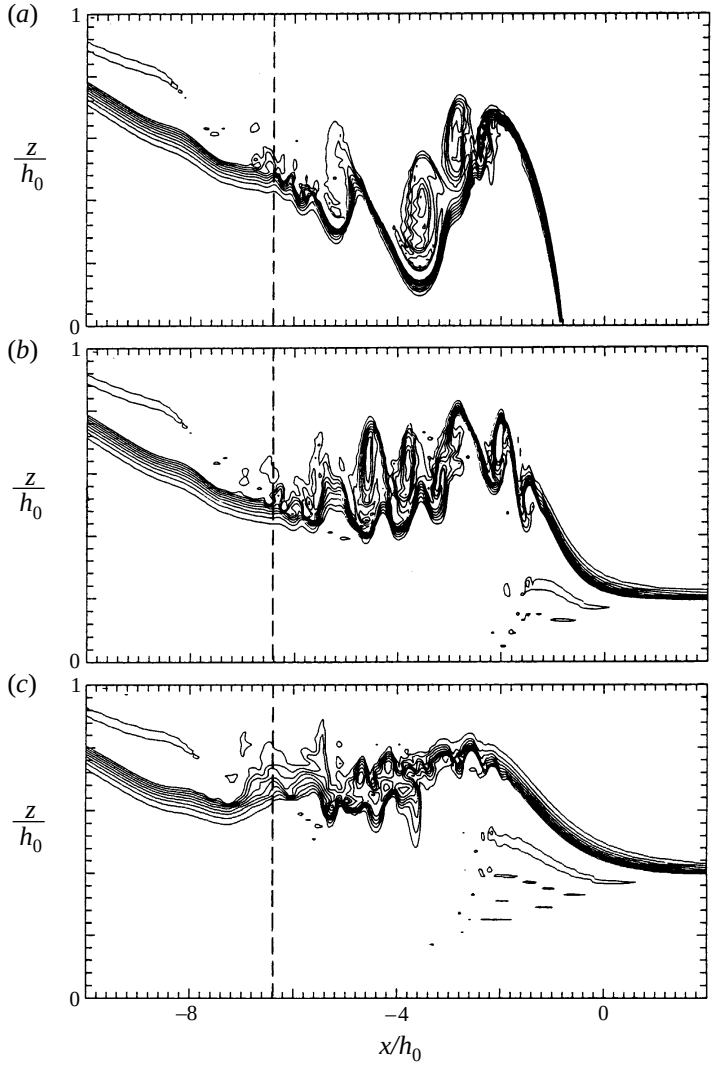

FIGURE 9. Simulated two-dimensional potential temperature field at $\hat{t} = 8$ in the dam-break problem for $h_0/d = 0.25$ and $h_a/h_0 =$ (*a*) 0, (*b*) 0.2, (*c*) 0.4. The contour interval is 1 K. – – –, Location of the leading edge of the initial reservoir.

5. Internal jumps with shear

The nature of the energy loss within an internal bore may differ from that in a classical hydraulic bore owing to differing vorticity characteristics within the bore. In a Boussinesq fluid, the pressure gradient is nearly vertical and the density gradient is normal to the interface between the layers such that baroclinic vorticity generation at the bore front produces counterclockwise circulation (in the perspective of figure 4) that turns the interface downstream as it passes through the bore. A similar behaviour occurs within the head of a gravity current, as is evident in comparing the bores depicted in figures 9(*b*) and 9(*c*) with the gravity-current head in figure 9(*a*). Turbulent mixing of the baroclinically generated velocity shear layer produces a velocity deficit near the interface in the contracting layer consistent with energy loss, while the opposite occurs in the expanding layer, as discussed in §3. On the other hand, in an

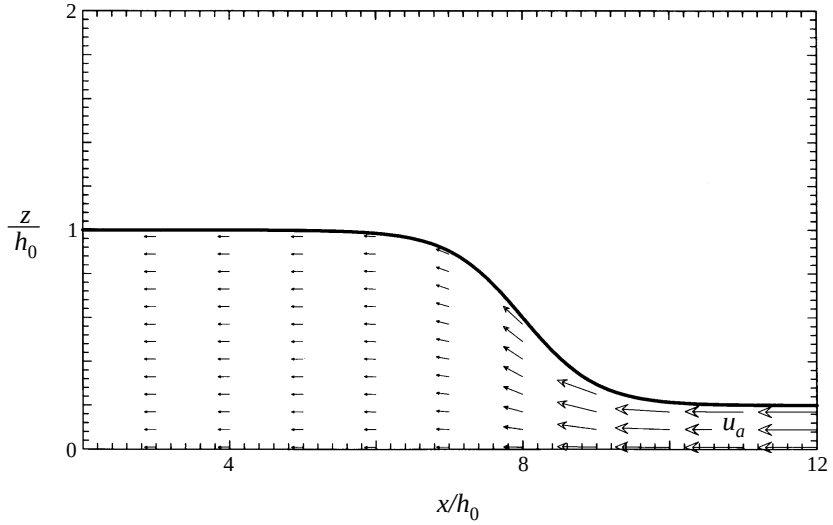

FIGURE 10. Initial flow field for two-dimensional numerical simulations of the dam-break problem with opposing flow beneath the inversion layer.

external bore forming along the free surface, the flow is highly non-Boussinesq and the direction of the pressure gradient may turn sufficiently far away from vertical that baroclinic vorticity production creates clockwise circulation (in the perspective of figure 5) in which flow entering the bore curls back on itself (Yeh 1991). Strong turbulence arises within the layer in the vicinity of the leading edge that mixes this circulation and produces a velocity deficit near the free surface that is consistent with the energy losses discussed in §3.

When shear is present in the flow ahead of the bore, there is an additional source of vorticity that may significantly alter the structure of the bore. If the flow speed beneath the inversion is greater than the flow aloft, the vorticity swept into the bore opposes the baroclinically generated vorticity, and if sufficiently strong, may cause the leading edge of the bore to curl forward and break back on itself, as occurs in the classical hydraulic system. In laboratory experiments, Wood & Simpson (1984) documented that internal jumps forming in the accelerated flow beneath the inversion in the lee of a towed obstacle exhibit turbulence that begins at the leading edge of the bore.

Within the context of the dam-break problem, we can investigate the influence of shear ahead of the jump in our two-dimensional non-hydrostatic model by including an opposing velocity in the initial flow beneath the inversion, as depicted in figure 10. To maintain the analogy with the shallow-water system, the horizontal flow is initially constant with height below the inversion, producing an initial velocity discontinuity across the inversion layer. The initial inversion surface (dam) has a sloping leading edge and the vertical velocity beneath the inversion is specified to maintain mass continuity. For the simulations presented here, $h_0 = 5$ km to the left of the sloping portion of the inversion surface, and $h_a = 1$ km to the right. To eliminate any effects of a finite channel depth, we place the top of the domain at 200 km, and employ a stretched grid in the vertical above 10 km.

The model domain translates to the right at a constant speed chosen such that the jump remains nearly stationary during the integration. As the integration proceeds, the shear layer ahead of the jump broadens slowly with time owing to the small background diffusion in the model. This layer will develop Kelvin–Helmholtz

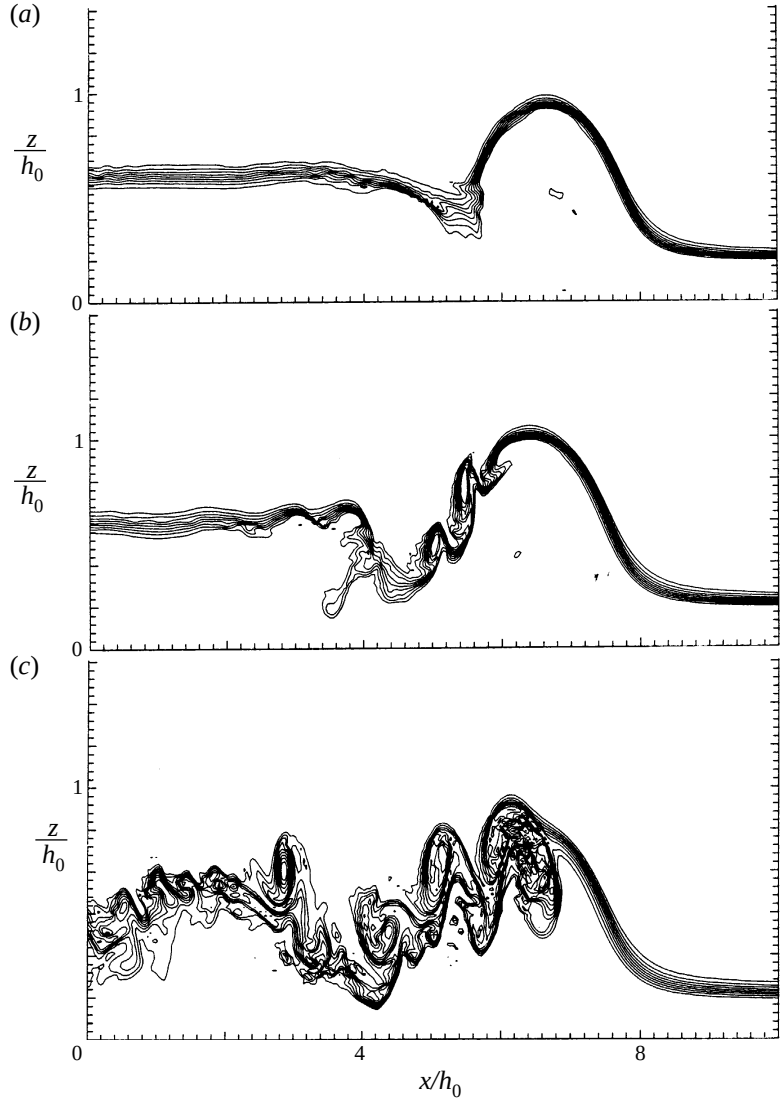

FIGURE 11. Two-dimensional simulation of the dam-break problem with an inversion layer ahead of the dam and an opposing flow of $u_a/(g'h_0)^{1/2} = -0.25$ beneath the inversion. (*a*) $\hat{t} = 15$; (*b*) 21; (*c*) 34.

instabilities even without the presence of the jump, but simulations with the dam removed confirm that the instability does not visibly alter the inversion surface until it is well beyond the point where the jump is located when the dam is present.

The structure of the jump that evolves upon 'release' of the dam with an opposing flow of $u_a = -10$ m s^{-1} ($u_a/(g'h_0)^{1/2} = -0.25$) is illustrated at three representative times in figure 11. In this simulation, the head of the jump is deeper and turbulence behind the head develops much more slowly than in the case with no ambient shear (cf. figure 9*b*). The opposing vorticity in the shear layer ahead of the jump promotes deeper lifting within the jump because it balances much of the baroclinically generated circulation near the leading edge (Rotunno, Klemp & Weisman 1988). This ambient vorticity also weakens the shear instability behind the head and delays the onset of

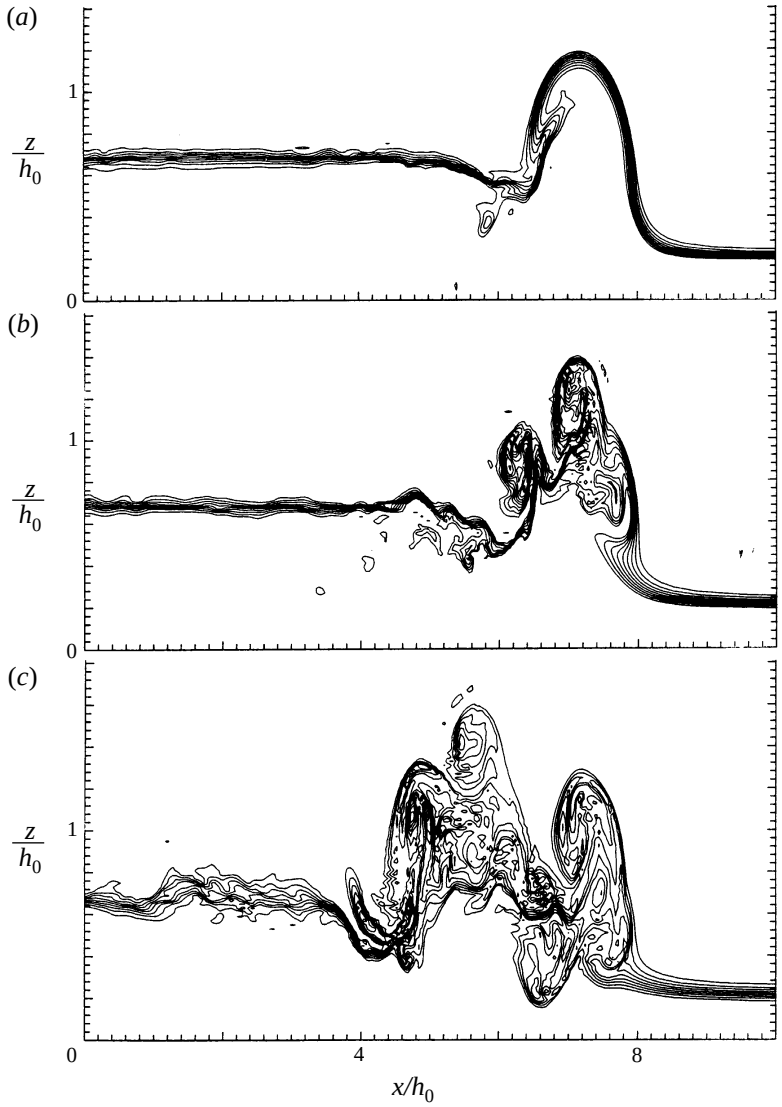

FIGURE 12. As in figure 11 except for $u_a/(g'h_0)^{1/2} = -0.5$.

K–H instability. At later times, the structure of the jump is again qualitatively similar to the head of a density current.

When the opposing flow is increased to $u_a/(g'h_0)^{1/2} = -0.5$ (shown in figure 12), the early development of the jump is similar to the $u_a/(g'h_0)^{1/2} = -0.25$ case. The height of the jump is even greater as the ambient shear and baroclinically generated vorticity appear to be more nearly in balance. However, shortly after eddies with negative (counterclockwise) vorticity begin to form behind the head (figure 12*a* at $\hat{t} = 15$), the leading edge begins to roll up, forming eddies of positive vorticity that collapse forward into the inversion layer (figure 12*b* at $\hat{t} = 21$). This behaviour persists at later times, with positive circulation dominating at the leading edge and negative circulation further above and behind the head.

Further increasing the opposing flow to $u_a/(g'h_0)^{1/2} = -0.75$ (figure 13), forward overturning dominates the turbulent breakdown at the leading edge of the jump

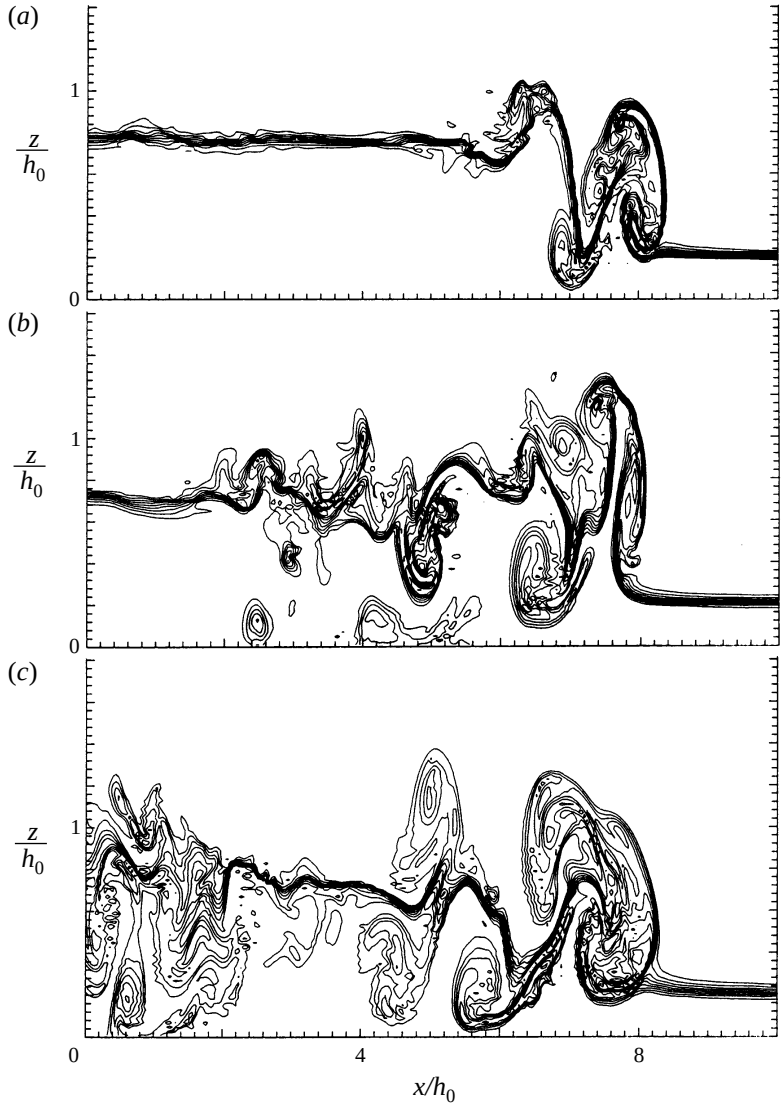

FIGURE 13. As in figure 11 except for $u_a/(g'h_0)^{1/2} = -0.75$. (*a*) $\hat{t} = 11$; (*b*) 19; (*c*) 30.

throughout the simulation. Successive eddies curl forward over the inversion layer and then descend through the inversion, sinking to the surface as they are swept to the rear. At $\hat{t} = 30$, a new vortex is rolling up at the leading edge while two previously formed vortices are clearly visible near the surface further to the rear. Thus, when the shear ahead of the jump is sufficiently strong to induce forward overturning, turbulent mixing rapidly penetrates throughout the lower layer, in marked contrast to the behaviour in the absence of shear in which turbulence is confined to a mixing zone between the two layers behind the head of the bore.

The differing character of the jump in the presence of strong shear is also evident in its propagation speed, which is displayed in figure 14 as a function of u_a. These front speeds can be compared with the theoretical behaviour in a one-layer shallow-water system with the appropriate reduced gravity g'. Including a velocity $u_a < 0$ beneath the

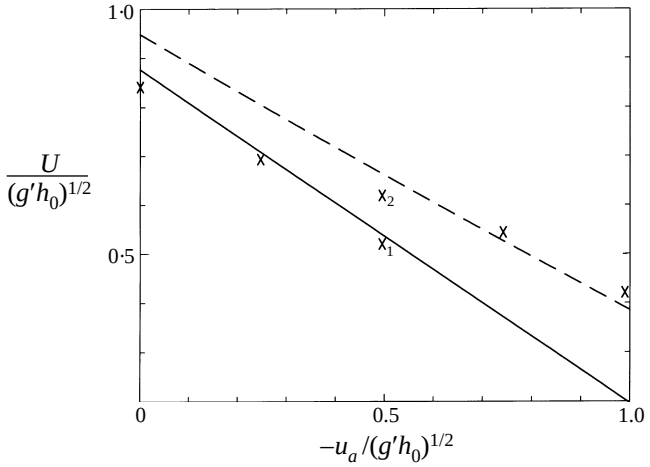

FIGURE 14. Propagation speed of the jump in the modified dam-break problem initiated with a mean flow u_a beneath the inversion as depicted in figure 10. The theoretical front speed based on the one-layer shallow-water equations is also displayed, assuming that the energy loss occurs either ——, above the SWL or – – –, within the layer.

inversion ahead of the dam, the equation for the rightward-propagating characteristic (28) is modified to:

$$\frac{h_a}{h_0}u_a + 2(g'h_0)^{1/2} = \beta u_a + (1-\beta)\,U + 2(g'h_f)^{1/2}. \tag{34}$$

Similarly, the front condition arising from the flow-force balance (2) as $d \to \infty$ now reduces to

$$U = u_a + k(g'h_f)^{1/2}, \tag{35}$$

where, as before, k is given by (31) assuming the energy loss occurs above the SWL, and by (32) if energy loss occurs within the SWL. Solving (34) together with (35) and either (31) or (32) defines the speed of the front as a function of u_a, which is also plotted in figure 14. For the smaller values of u_a, the structure of the jump is similar to the internal bore and the front speeds compare well with the shallow-water theory assuming energy loss occurs above the SWL. When u_a is large enough to reverse the circulation due to baroclinic forcing at the leading edge and cause the front to curl forward and collapse back on itself, the front speeds are in better agreement with the classical shallow-water theory in which energy loss is confined to the SWL. For $u_a/(g'h_0)^{1/2} = -0.5$, two front speeds are plotted; $\times_1$ was estimated prior to $\hat{t} = 15$ while the front resembled an internal bore, while $\times_2$ was taken after the forward overturning was well established. Thus, the front speeds up and moves toward the classical theory as the circulation at the leading edge is reversed.

To further illustrate the differing behaviour that may arise in internal jumps and bores, we computed the time-averaged fields in the two-dimensional simulations over a period from $\hat{t} = 15$ to 45 in a coordinate framework in which the jump or bore is essentially stationary. Figure 15(*a*) depicts the time-averaged potential temperature $\bar{\theta}$ for the internal bore ($u_a = 0$) and suggests that mixing of the inversion layer begins well behind the leading edge and broadens to the rear through mixing across the unstable shear layer. We have attempted to estimate the distribution of the rate of energy loss

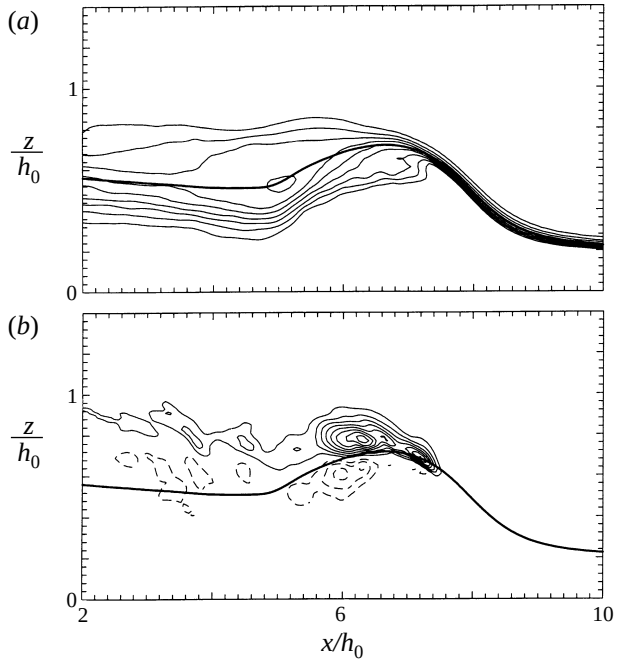

FIGURE 15. Time-averaged flow between $\hat{t} = 15$ and 45 for the two-dimensional simulation of the dam-break problem with an inversion layer ahead of the dam (same simulation as in figure 11 except $u_a = 0$). (*a*) Potential temperature field with 1 K contour interval. (*b*) Rate of energy loss per unit mass due to turbulent stress E_m with a contour interval of $0.02g'^{3/2}h_0^{1/2}$. – – –, negative contours (indicating energy gain), and the zero line is omitted. ——, Location of the time-averaged streamline separating two the layers ahead of the bore.

E_m per unit mass owing to turbulent stresses within the bore from the time-averaged fields according to:

$$E_m = -\bar{\boldsymbol{V}}\cdot\left\{\bar{\boldsymbol{V}}\cdot\boldsymbol{\nabla}\bar{\boldsymbol{V}} = c_p\,\theta_2\,\boldsymbol{\nabla}\bar{\pi} - g\frac{\bar{\theta}-\theta_2}{\theta_2}\hat{\boldsymbol{k}}\right\}, \tag{36}$$

where $\bar{\boldsymbol{V}} = (\bar{u}, \bar{w})$, π is the perturbation Exner function, $\hat{\boldsymbol{k}}$ is the vertical unit vector, and overbars denote time-averaged variables.

The spatial distribution of E_m for the time-averaged bore is displayed in figure 15(*b*). This figure suggests that energy change is confined to the mixing zone extending behind the head of the bore, with energy loss concentrated just above the mean streamline dividing the two streams, and weaker energy gain below the dividing streamline. This result is consistent with our idealized analysis in §3 of a bore with localized mixing within each layer.

When the shear between the layers is sufficiently strong to reverse the direction of overturning within the jump, the structure of the time-averaged fields, shown in figure 16 for $u_a/(g'h_0)^{1/2} = -0.75$, is very different. Strong mixing of potential temperature extends throughout the entire head region of the jump (figure 16*a*), and the mean streamline separating the two layers reflects the forward overturning occurring within the head. The energy loss (figure 16*b*) is concentrated within the lower layer beneath the head of the jump, with only weak energy loss in the upper layer above the head. This behaviour is qualitatively similar to that expected in classical hydraulic jumps, in which all of the energy loss must occur within the lower layer.

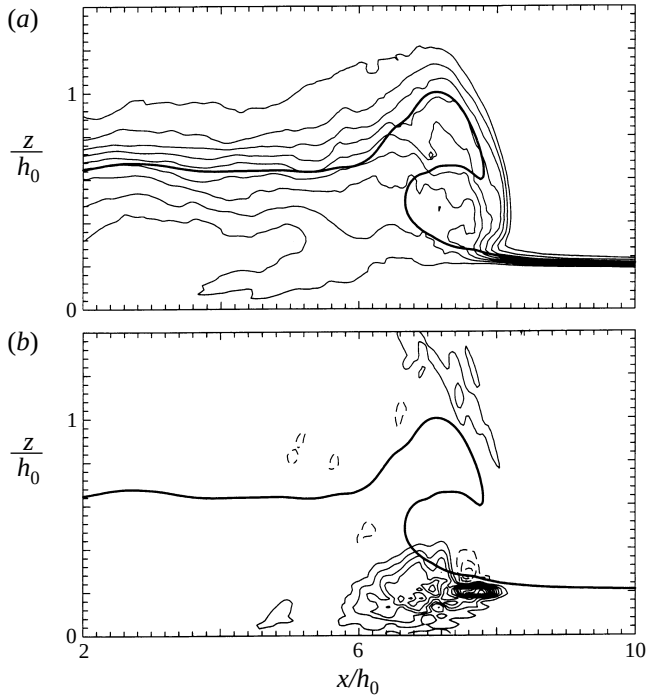

FIGURE 16. Time-averaged flow, as in figure 15, except for the simulation shown in figure 13 with $u_a/(g'h_0)^{1/2} = -0.75$ and the contour interval in (*b*) is $0.04g'^{3/2}h_0^{1/2}$.

While there is no fundamental difference between hydraulic jumps and bores in classical hydraulic theory, these simulations suggest that when internal jumps form along an inversion layer in the presence of strong shear, their structure and propagation may differ substantially from internal bores. The additional source of vorticity in the inversion layer opposes the baroclinic generation, and if sufficiently strong, may reverse the circulation at the front and create eddies that penetrate to the surface and increase the turbulent mixing within the lower layer. In this situation, the theory that follows the classical approach in assuming energy loss is confined to the lower layer may be appropriate.

6. Flow over an obstacle

The distinction between internal bores and hydraulic jumps may also be important in characterizing the internal structure of flow over obstacles. When a two-layer Boussinesq fluid flows over an obstacle, internal shocks may form both upstream and downstream of the barrier as illustrated in figure 17. The behaviour of these jumps has traditionally been described through analogy with hydraulic flow using the shallow-water equations with a suitably reduced gravity (cf. Long 1954; Houghton & Kasahara 1968). Through analysis of the steady one-layer shallow-water equations along with the classical hydraulic jump conditions that conserve mass and momentum within the SWL, Houghton & Kasahara (1968) determined the characteristics of these shocks as a function of the ambient Froude number $F = u_0/(g'h_0)^{1/2}$ and the normalized obstacle height $M = h_c/h_0$. They found that upstream bores, together with hydraulic jumps in the lee, form when these parameters fall within the envelope enclosed by the heavy solid line in figure 18(*a*). Within this regime, the bore forming ahead of the obstacle

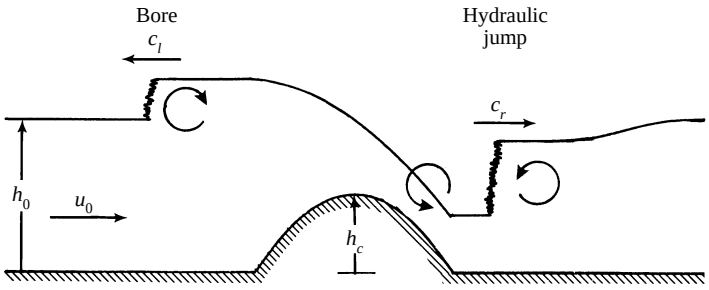

FIGURE 17. Schematic of shallow-water flow over a barrier depicting the upstream-propagating bore and downstream-propagating jump.

propagates at a steady speed $c_l < 0$ upstream relative to the obstacle, as indicated in figure 18(*a*). Baines & Davies (1980) noticed that the theory indicates these windward bores continue to propagate upstream until the Froude number reaches the heavy dashed line in figure 18(*a*). Thus, they described the regime between the upper heavy solid curve and the heavy dashed curve as a hysteresis zone in which the flow could either remain everywhere supercritical or produce upstream propagating bores, depending on the specific nature of the transient evolution.

In light of the evidence presented in the previous sections, the behaviour of internal bores propagating ahead of the obstacle may be alternatively described using the front condition (11), in which energy is conserved within the SWL. In fact, in the laboratory experiments that demonstrate good agreement with (11) in figures 2 and 3, the internal bores were generated ahead of an obstacle towed through a channel.

Rederiving Houghton & Kasahara's (1968) profiles in figure 18(*a*), but using the front condition (14) that conserves energy within the SWL instead of hydraulic relation (4), produces the modified diagram displayed in figure 18(*b*). The curve that bounds the regions in which the flow is everywhere subcritical or everywhere supercritical is given by:

$$M = 1 + \tfrac{1}{2}F^2 - \tfrac{3}{2}F^{2/3}, \tag{37}$$

the same as in figure 18(*a*). The blocked region is bounded by the curve:

$$F^2 = \frac{2(M-1)^2}{M+1}, \tag{38}$$

which differs slightly from the corresponding curve in figure 18(*a*). However, the curves depicting the speed of the upstream-propagating bore differ noticeably from their behaviour in figure 18(*a*). In particular, the conditions in which the upstream bore just becomes stationary ($c_l = 0$) coincide exactly with the boundary for everywhere supercritical flow (37). Thus, the hysteresis zone that arises in hydraulic theory (figure 18*a*), disappears for internal bores that conserve energy within the SWL. Baines (1984) sought to verify the existence of multiple states within the hysteresis zone in the laboratory by establishing an upstream-propagating bore with F below the critical curve and then increasing the speed of the towed obstacle to raise F above the critical curve. In these experiments, upstream bores could be maintained only in the lower portion of this zone, which Baines attributed to the influence of interfacial drag in reducing the bore speed. However, our modified theory for internal bores suggests that Baines' partial confirmation of the hysteresis zone could be due to non-Boussinesq influences in his experiments.

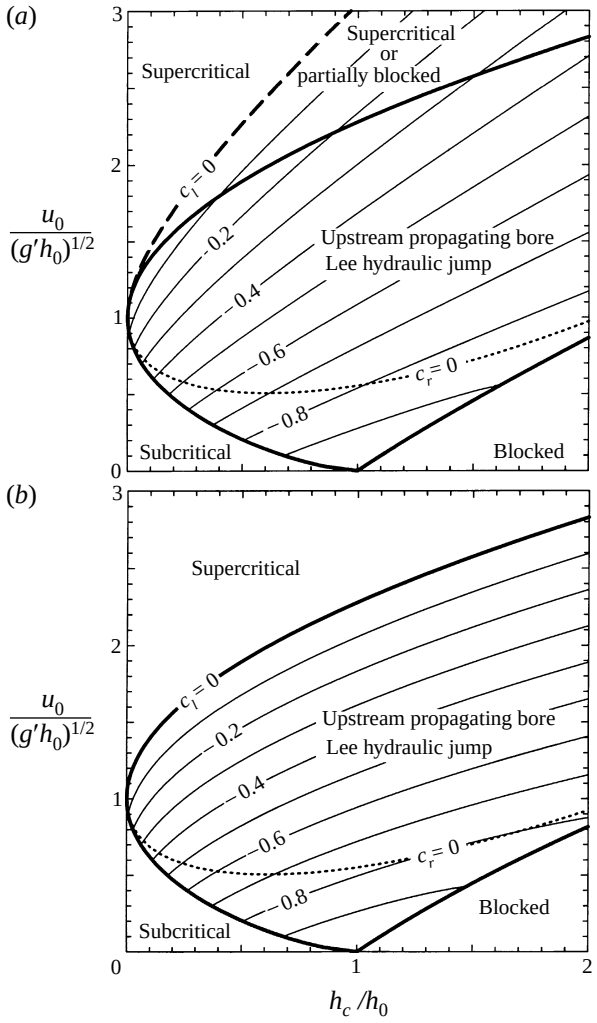

FIGURE 18. Froude number regime diagram for shallow-water flow over an obstacle. (*a*) Curves from Houghton & Kasahara (1968) with the traditional hydraulic jump condition applied to the upstream bore. The heavy solid line encloses the region in which upstream bores and lee hydraulic jumps form. The thin solid lines reflect the speed of the upstream-propagating bore, and the dotted line marks the boundary between stationary (below) and downstream-propagating (above) lee hydraulic jumps. The heavy-dashed line represents a modification to the regime of bore formation identified by Baines & Davies (1980). (*b*) Modified regime diagram assuming that the upstream-propagating internal bore conserves energy within the SWL.

Within the envelope of the heavy solid line in figure 18, hydraulic jumps form in the lee, as illustrated in figure 17. However, these internal lee jumps may differ in character from the internal bore forming ahead of the obstacle. Laboratory experiments in which an obstacle is towed beneath a Boussinesq fluid reveal that turbulence begins at the leading edge of the lee jump (cf. Long 1954; Wood & Simpson 1984), while in the upstream propagating internal bore, turbulence first appears behind a head that is visually similar to a gravity current or the first crest of an undular oscillation (cf. Rottman & Simpson 1989). Strong shear, present just above the supercritical flow beneath the inversion in the lee of the obstacle, promotes forward overturning in the

lee jumps (cf. Rotunno & Smolarkiewicz 1995), similar to the idealized simulation shown in figure 13. Thus, we expect that the lee internal jumps might be best characterized by the classical hydraulic jump conditions.

Applying the traditional hydraulic jump conditions (conservation of mass and momentum within the SWL) to the lee jump shown in figure 17, Houghton & Kasahara (1968) found that jumps forming in conditions falling below the dotted line ($c_r = 0$) in figure 18(*a*) remain stationary on the lee slope of the obstacle, while for Froude numbers above this line, lee jumps propagate steadily downstream. These results appear to be consistent with the behaviour observed in laboratory experiments (cf. Long 1954). Using this momentum-conserving front condition (4) for the lee jump together with the energy-conserving condition (14) for the upstream bore, the $c_r = 0$ curve separating the stationary and propagating jump regimes (shown in figure 18*b*), is only slightly altered from Houghton & Kasahara's result. If the energy-conserving front condition is also applied to the lee jump, the theory would predict that all lee jumps propagate downstream, which is contrary to their observed behaviour.

7. Summary

Hydraulic theory has been successfully applied to a variety of flow situations, often producing simple conceptual and/or quantitative relations that capture the essence of the more complex physics. We have found that by altering the traditional conservation requirements, hydraulic theory provides a more accurate description of internal bore propagation, particularly for bores approaching the gravity-current ($h_a \to 0$) limit. In applying shallow-water theory to internal bores, this modification requires that energy rather than momentum be conserved within the SWL across the bore. Momentum conservation within the SWL is no longer required since momentum adjustment also takes place in the fluid above the SWL.

The differing behaviour of internal bores and hydraulic bores forming along a free surface may result from the differing structure of the head region of the bore. Turbulent bores propagating along a free surface develop a circulation that causes their leading edge to curl forward, producing turbulent eddies that penetrate back into the lower fluid layer. This circulation creates a velocity profile that decreases with height, exhibiting a positive velocity deficit (see equation (18)) that produces energy loss according to the idealized analysis in §3. For internal bores forming in a Boussinesq fluid along an interface containing a step change in density or potential temperature, strong baroclinic vorticity generation in the head region (in the opposite direction to that arising in a free-surface bore) sweeps flow near the interface to the rear, such that turbulence forms through Kelvin–Helmholtz instability behind the head. In this situation, flow beneath the interface is accelerated by shear stresses owing to the faster moving fluid aloft, producing a negative velocity deficit that corresponds to energy gain according to the analysis in §3. Two-dimensional non-hydrostatic simulations in §5 provide further evidence that energy loss within internal bores occurs primarily in the region above the mean streamline dividing the two layers, with weaker energy gain below.

The assumption that energy is conserved within the expanding layer beneath a propagating internal bore is clearly a gross simplification of the actual dynamic structure. The application of shallow-water theory to internal bores is also problematic because of the mixing that occurs across the interface initially separating the layers of differing density. Nevertheless, the assumption that energy is conserved within the SWL is physically more plausible than the reverse assumption of energy conservation

above the SWL, and appears to provide a simple expression for internal bore propagation that is reasonably accurate over a broad range of conditions.

The simplicity of the front condition is particularly useful in numerical shallow-water models, where the numerical techniques used in solving the equations may directly control the behaviour of propagating bores. For example, in a one-layer shallow-water model solved in advective form (with u and h as prognostic variables), numerically integrating the equations across the front of a bore is equivalent to imposing the energy-conserving front condition (14). However, if the equations are integrated using the momentum form (with uh and h as prognostic variables), the resulting momentum-conservation across steadily propagating bores will produce behaviour consistent with the classical front condition (4).

In classical hydraulic theory for flow with a free upper surface, there is no fundamental difference between a bore and a hydraulic jump. However, as demonstrated in § 5, with the presence of strong shear in the inversion layer, internal hydraulic jumps may develop characteristics very different from those of an internal bore. If vorticity associated with the shear is sufficiently strong, circulation near the leading edge may be reversed, with the result that the jump behaves more like that described by classical hydraulic theory. When flow containing an internal inversion layer passes over an obstacle, both an upstream propagating bore and a lee hydraulic jump may be simultaneously produced having these differing properties.

This research is supported in part by the Office of Naval Research grant No. N00014-94-F-0032. The National Center for Atmospheric Research is sponsored by the National Science Foundation.

REFERENCES

Baines, P. G. 1984 A unified description of two-layer flow over topography. *J. Fluid Mech.* **146**, 127–167.

Baines, P. G. 1995 *Topographic Effects in Stratified Flows*. Cambridge University Press.

Baines, P. G. & Davies, P. A. 1980 Laboratory studies of topographic effects in rotating and/or stratified fluids. GARP Pub. Ser. 23, *Orographic Effects in Planetary Flows*, ICSU/WMO, pp. 233–299.

Batchelor, G. K. 1967 *An Introduction to Fluid Mechanics*. Cambridge University Press.

Benjamin, T. B. 1968 Gravity currents and related phenomena. *J. Fluid Mech.* **31**, 209–248.

Chu, V. H. & Baddour, R. E. 1977 Surges, waves and mixing in two-layer density stratified flow. *Proc. 17th Congr. Intl Assn Hydraul. Res.* vol. 1, pp. 303–310.

Clark, R. H., Smith, R. K. & Reid, D. G. 1981 The Morning Glory of the Gulf of Carpentaria: an atmospheric undular bore. *Mon. Weather Rev.* **109**, 1726–1750.

Dorman, C. E. 1987 Possible role of gravity currents in Northern California's coastal summer wind reversals. *J. Geophys. Res.* **92**, 1497–1506.

Haase, S. P. & Smith, R. K. 1984 Morning Glory wave clouds in Oklahoma: a case study. *Mon. Weather Rev.* **112**, 2078–2089.

Hager, W. H. & Bremen, R. 1989 Classical hydraulic jumps. *J. Hydraul. Res.* **27**, 565–585.

Hermann, A. J., Hickey, B. M., Mass, C. M. & Albright, M. D. 1990 Orographically trapped coastal wind events in the Pacific Northwest and their oceanic response. *J. Geophys. Res.* **95**, 13169–13193.

Hornung, H. G., Willert, C. & Turner, S. 1995 The flow field downstream of a hydraulic jump. *J. Fluid Mech.* **287**, 299–316.

Houghton, D. D. & Kasahara, A. 1968 Nonlinear shallow fluid flow over an isolated ridge. *Commun. Pure. Appl. Maths* **21**, 1–23.

KLEMP, J. B., ROTUNNO, R. & SKAMAROCK, W. C. 1994 On the dynamics of gravity currents in a channel. *J. Atmos. Sci.* **269**, 169–198.

LANDAU, L. D. & LIFSHITZ, E. M. 1959 *Fluid Mechanics*. Pergamon.

LONG, D., RAJARATNAM, N., STEFFLER, P. M. & SMY, P. R. 1991 Structure of flow in hydraulic jumps. *J. Hydraul. Res.* **29**, 207–218.

LONG, R. R. 1954 Some aspects of the flow of stratified fluids, II. Experiments with a two-fluid system. *Tellus* **6**, 97–115.

PRANDTL, L. & TIETJENS, O. G. 1934 *Applied Hydro- and Aeromechanics*. Dover.

ROTTMAN, J. W. & SIMPSON, J. E. 1983 Gravity currents produced by instantaneous releases of a heavy fluid in a rectangular channel. *J. Fluid Mech.* **135**, 95–110.

ROTTMAN, J. W. & SIMPSON, J. E. 1989 The formation of internal bores in the atmosphere: A laboratory model. *Q. J. R. Met. Soc.* **115**, 941–963.

ROTUNNO, R., KLEMP, J. B. & WEISMAN, M. L. 1988 A theory for long-lived squall lines. *J. Atmos. Sci.* **45**, 463–485.

ROTUNNO, R. & SMOLARKIEWICZ, P. K. 1995 Vorticity generation in the shallow-water equations as applied to hydraulic jumps. *J. Atmos. Sci.* **52**, 320–330.

SCHIJF, J. B. & SCHÖNFELD, J. C. 1953 Theoretical considerations on the motion of salt and fresh water. *Proc. Minn. Intl Hydraulics Conv.* University of Minnesota, pp. 321–333.

SCHREFFLER, J. H. & BINOWSKI, F. S. 1981 Observations of pressure jump lines in the Midwest, 10–12 August 1976. *Mon. Weather Rev.* **109**, 1713–1725.

SIMPSON, J. E. & BRITTER, R. E. 1979 The dynamics of the head of a gravity current advancing over a horizontal surface. *J. Fluid Mech.* **94**, 477–495.

STOKER, J. J. 1957 *Water Waves*. Interscience.

TURNER, J. S. 1973 *Buoyancy Effects in Fluids*. Cambridge University Press.

WOOD, I. R. & SIMPSON, J. E. 1984 Jumps in layered miscible fluids. *J. Fluid Mech.* **140**, 329–342.

YEH, H. H. 1991 Vorticity-generation mechanisms in bores. *Proc. R. Soc. Lond.* A **423**, 215–231.

YIH, C. S. & GUHA, C. R. 1955 Hydraulic jump in a fluid system of two layers. *Tellus* **7**, 358–366.